A Journal of the Gesellschaft Deutscher Chemiker

Angewandte International Edition GDCh Chemie

www.angewandte.org

Accepted Article

Title: Artificial Lithium Channels Built from Polymers with Intrinsic Microporosity

Authors: Fei Gou, Qiuting Wang, Zihong Yang, Wenju Chang, Jie Shen, and Huaqiang Zeng

To be cited as: *Angew. Chem. Int. Ed.* **2024**, e202418304

Link to VoR: https://doi.org/10.1002/anie.202418304

WILEY VCH

10.1002/anie.202418304

WILEY-VCH

Research Communications

PIM-Based Li^+ Channels

DOI: 10.1002/anie.200((will be filled in by the editorial staff))

Artificial Lithium Channels Built from Polymers with Intrinsic Microporosity

Fei Gou, Qiuting Wang, Zihong Yang, Wenju Chang, Jie Shen and Huaqiang Zeng**

Abstract: *In sharp contrast to numerous artificial potassium channels developed over the past decade, the study of artificial lithium-transporting channels has remained limited. We demonstrate here the use of an interesting class of polymers with intrinsic microporosity (PIM) for constructing artificial lithium channels. These PIM-derived lithium channels show exceptionally efficient (γ_{Li}^+ > 40 pS) and highly selective transport of Li^+ ions, with selectivity factors of > 10 against both Na^+ and K^+. By simply adjusting the initial reaction temperature, we can tune the transport property in a way that PIMs synthesized at initial reaction temperatures of 60 °C and 80°C exhibit improved transport efficiency and selectivity, respectively, in the dioleoyl phosphatidylcholine membrane.*

Cation-transporting channels, essential transmembrane proteins in nature, play critical role in processes such as nerve conduction, muscle contraction, and cell division.[1-2] Malfunctions or structural alterations in these proteins can disrupt cellular ion balances, resulting in disorders like familial febrile seizures, long QT syndrome, and hyperkalemia.[3] While advancements in structural biotechnology have led to significant insights into these channel proteins,[4-6] their complex structures and dependence on specific bilayer membrane have limited their practical applications. In contrast, biomimetic artificial cation channels feature simpler and more accessible structures. These artificial versions not only enhance our understanding of ion transport mechanisms but also expand the potential applications of membrane transport in fields such as biology, medicines and sensing. [7-23]

Nevertheless, current artificial systems are far less selective in ion transport with respect to their natural counterparts. For instance, natural potassium channels can selectively transport K^+ 1000 times as fast as Na^+.[24] Yet, the best artificial K^+ channels achieve only a K^+/Na^+ selectivity factor of 20.1.[25-26] Consequently, developing highly selective artificial cation transmembrane channels remains a constant challenge, particularly for those that can seamlessly integrate high transport selectivity with high transport efficiency.

In recent years, the constructions of artificial transmembrane channels using polymeric molecules has clearly become one of promising research directions in the field.[27-41] These polymeric backbones can be classified into two types, one featuring a random coil structure,[27-29] and the other derived from highly rigid foldamer molecules with long-range order.[30-41] As a result, opportunities and challenges lie ahead in developing diverse types of polymeric backbones for the design of innovative channel systems.

Polymers with Intrinsic Microporosity (PIMs) are a class of amorphous organic polymers built from monomers that often have a rigid and non-linear structure. The rigidity and contortion within these building blocks prevent the polymeric chains from packing closely, leading to a high free volume and micropores generally less than 2 nm in diameter.[42-44] In a sense, the backbone rigidity of PIMs is intermediate between the randomized coil conformation[27-29] and the highly ordered rigid folding backbones.[30-41] Since the first report of PIMs by Mckeown in 2004,[45] a range of PIM-based applications have been demonstrated including catalysis, sensors and chiral separations due to their simple synthesis, good solubility, excellent film-forming abilities.[46-48] Especially in the making of membrane materials for gas separation, it has shown unparalleled application potential and value.[49-53] As a class of intrinsically porous materials with excellent properties, PIMs have numerous other potential applications that are yet to be fully explored. To the best of our knowledge, there have been no report of their use in developing artificial transporters functioning within lipid bilayer membranes.

Here, we designed and synthesized a unique type of polyimide-based PIMs (**PIM-PI**) readily prepared by the facile “one-pot” polymerization via condensing dianhydride and diamine building blocks (Figure 1a and Scheme S1). And we have investigated their ion transport properties within lipid bilayer membranes. Notably, the optimized **PIM-PI**s exhibit exceptionally high Li^+ transmembrane transport activity, with a conduction rate exceeding 40 pS, along with high transport selectivity factors of > 14.3 toward Na^+ and > 10.5 toward K^+. As far as we know, these **PIM-PI** channels represent the fastest artificial Li^+ channel, forming a third class of artificial Li^+ channel, following two previously established foldamer-based channel systems based on a H-bonded folding nanotube[39] and self-assembled short helices.[54]

Among the diverse types of PIMs, we chose to work with polyimides because the presence of imide groups, as we hypothesized, may aid in efficient capture and transport of cations through the micropores (Figure 1a). Additionally, to improve biocompatibility and film-forming capabilities, we incorporated a flexible alkyl chain into the rigid PIM framework, generating

[*] Dr. F. Gou, Mrs. Q. Wang, Mr. Z. Yang, Dr. W. Chang, Prof. Dr. J. Shen and Prof. Dr. H. Zeng
College of Chemistry
Fuzhou University
Fuzhou, Fujian 350116, China
E-mail: hqzeng@fzu.edu.cn

Supporting information for this article is available on the WWW under: http://www.angewandte.org or from the author.

10.1002/anie.202418304

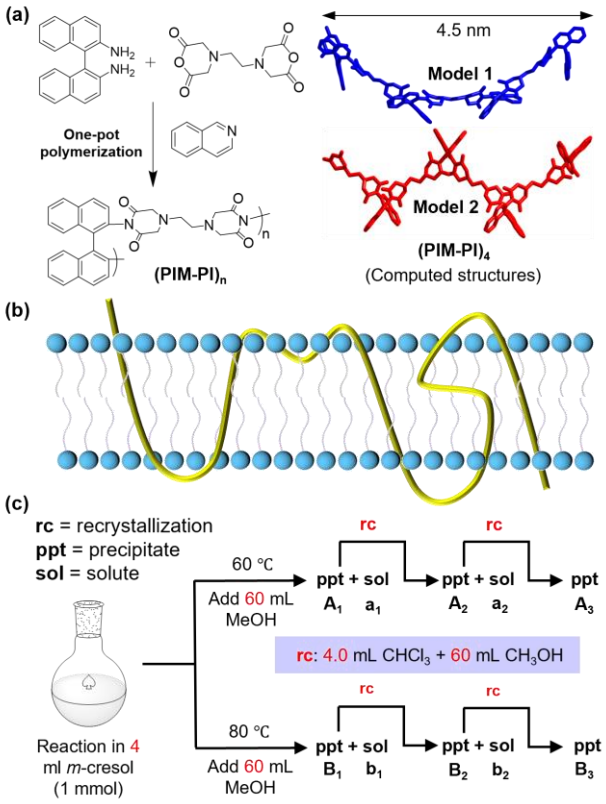

Figure 1 (a) One-pot preparation of AB-type **PIM-PI**s and two tetrameric oligomers geometrically optimized at the level of M06-2X/6-31+G(d), suggesting the existence of both curved and linear backbones in **PIM-PI**. (b) Schematic representation of **PIM-PI**s within a bilayer membrane, illustrating their role in facilitating ion transport across the membrane. (c) Purification protocols for **PIM-PI**s synthesized at two different initial reaction temperatures, 60 °C and 80 °C. Sequential purification steps yield six solid-phase products ($\mathbf{A_n}$ and $\mathbf{B_n}$) and four liquid-phase products ($\mathbf{a_n}$ and $\mathbf{b_n}$). For detailed conditions, see Table S1.

curved and linear backbone curvatures as depicted in models 1 and 2 computationally optimized at the level of M06-2X/631+G(d). Although numerous combinations involving these two sub-structural components could produce a variety of backbone designs, the rigidity and twisted nature of these substructures should hinder the polymer chains from packing tightly, potentially creating substantial free volume and intrinsic micropores to support efficient ion transport (Figure 1b).

These **PIM-PI** polymers were readily prepared using a previously established two-step procedure with slight modifications.[55] In the typical conditions, diamine (1.00 mmol) and dianhydride (1.00 mmol) were added to *m*-cresol (4 mL) under N_2 protection, which was heated to 60 °C (or 80 °C) for 1 h and then to 180 °C for 4 h. This was followed by adding methanol (60 mL) to precipitate out crude polymer products designated as **A** for 60 °C and **B** for 80 °C (Figure 1c and Table S1), respectively. These crude products were further purified twice by dissolving them in chloroform (40 mL) and precipitating from 40 mL methanol. This sequential purification process yielded $\mathbf{A_n}$ and $\mathbf{B_n}$(n= 1-3) as well as $\mathbf{a_n}$ and $\mathbf{b_n}$ (n = 1-2) (Figure 1b and Table S2).

We first recorded gel permeation chromatography (GPC) spectra, revealing one single sharp peak for both $\mathbf{A_n}$ and $\mathbf{B_n}$ (Figure 2a). The determined molecular weights show that the sequential purification process consistently gives rise to increasing enrichment of higher molecular weight polymers from 20.8 kD to 119.3 kD for $\mathbf{A_n}$, from 15.5 kD to 76.8 kD for $\mathbf{B_n}$, from 7.4 kD to 10.6 kD for $\mathbf{a_n}$ and from 8.4 kD to 11.4 kD for $\mathbf{b_n}$ series (Figure 2b and Table S3). This is reasonable since the low molecular weight organic polymers of this type may dissolve better in $CHCl_3$/MeOH solvent. Consistent with their polymeric nature, the corresponding NMR spectra of these polymers display several broad peaks (Figures S1-S4).

The ion recognition abilities of the PIMs $\mathbf{A_3}$ and $\mathbf{B_3}$ toward Li^+ metal ions via its imide oxygen atoms were measured by fluorescence titration experiments. We found that Li^+ ions elicit much larger fluorescence changes of $\mathbf{A_3}$ and $\mathbf{B_3}$ than both Na^+ and K^+ ions (Figure S5), suggesting that the PIM backbone interact with Li^+ more specifically.

We have also carried out computational molecular modelling at the level of B3LYP-D3/6-31G(d) to calculate the binding energy upon removing two or four water molecules from the hydrated Li^+, Na^+ and K^+ ions by one or two molecules of structural unit **1** (Eq. 1 and 2, Table S4 and Figures S6 and S7), which corresponds to the repeating unit of the PIM backbone.

Energetically, the binding of **1** to Na^+ is the most preferred, followed by Li^+ and K^+. Given the largest fluorescence change observed for Li^+ ion (Figure S5) and the subsequent experimental data that demonstrate Li^+ to be the most efficiently transported species (Figure 2), we speculate that the PIM backbone, which is relatively rigid, most likely binds the hydrated Na^+ ions in a manner that only two of its hydrated water molecules are released with a binding energy of -24.8 kcal/mol. Since Na^+ is not the favoured ion for transmembrane transport, the binding energy for Li^+ ion should be larger than -24.8 kcal/mol. That is, the PIM backbone shall be capable of simultaneously stripping four water molecules from Li^+ ion, releasing energies of -35.6 kcal/mol, -36.8 kcal/mol and -31.3 for 4-, 5-and 6-coordinated Li^+ ions, respectively. As the most stable hydrated Li^+ ions are 4-coordinate in aqueous solution,[56] we believe that the majority of Li^+ ions traverse through the membrane in a fully dehydrated form, with some ions retaining up to two water molecules.

The ion transport activities of the PIM polymers ($\mathbf{A_n}$, $\mathbf{B_n}$, $\mathbf{a_n}$ and $\mathbf{b_n}$) were evaluated by a vesicle-based kinetic HPTS assay, which utilizes a pH-sensitive HPTS dye within a DOPC-based bilayer membrane (Figure 2c). Using this assay, we observed increasingly active Li^+ transport activities from 26% for $\mathbf{A_1}$, 76% for $\mathbf{A_2}$ to 91% for $\mathbf{A_3}$ at 10 μg/ml and from 7.8% for $\mathbf{B_1}$, 46% for $\mathbf{B_2}$ to 82% for $\mathbf{B_3}$ at 25 μg/ml (Figure 2d,e), with activities ranging from 8% to 33% for $\mathbf{a_n}$ and $\mathbf{b_n}$ (Figure S8). These trends in transport activity correlate well with the enrichment trends in molecular weight determined by GPC analyses, suggesting that lower molecular weight polymers are less favourable for efficient Li^+ transmembrane transport. In addition, $\mathbf{A_n}$ series synthesized at an

10.1002/anie.202418304

WILEY-VCH

Research Communications

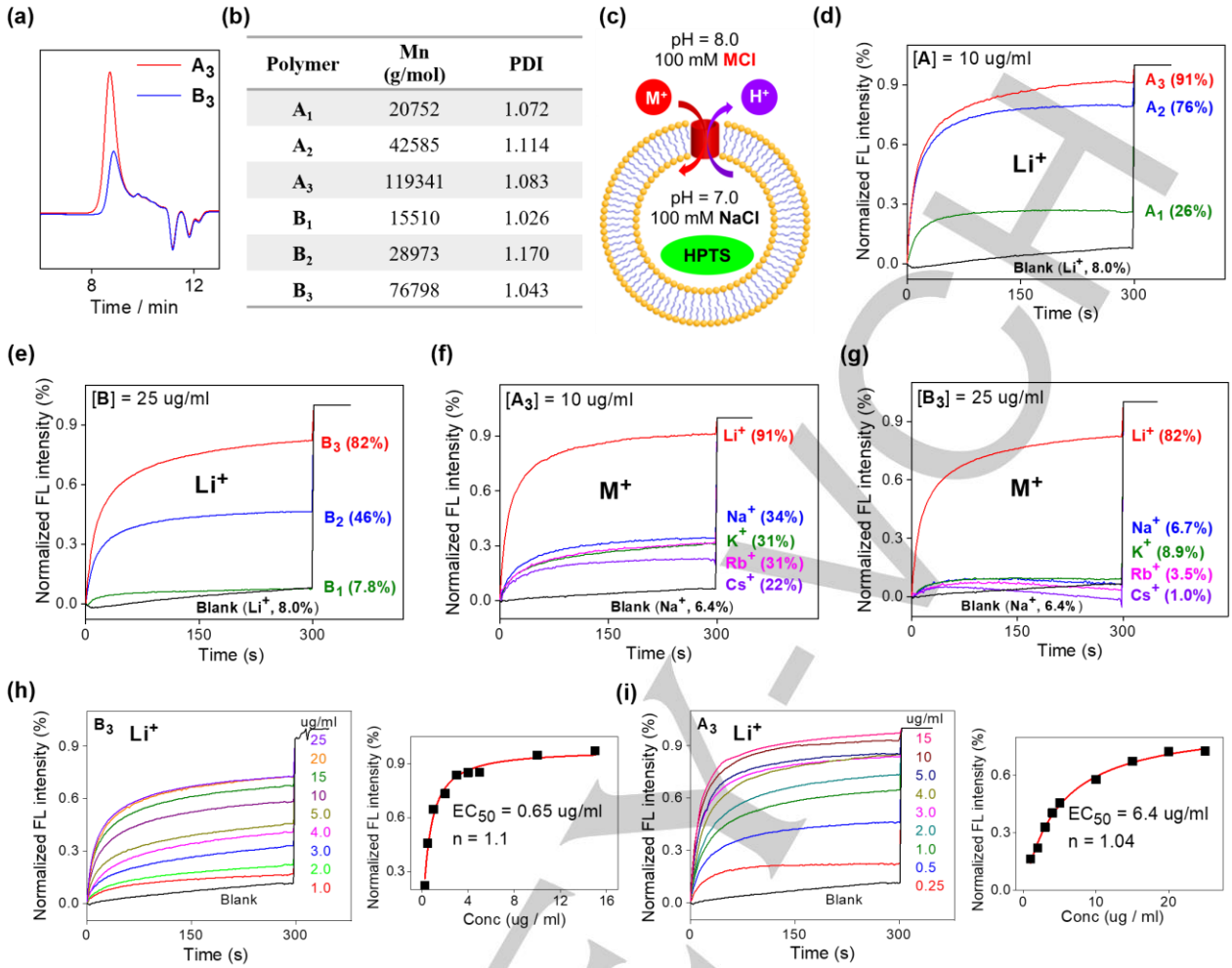

Figure 2. (a) and (b) present the GPC traces and molecular weights for the solid-phase products of $\mathbf{A_n}$ and $\mathbf{B_n}$, obtained through the sequential purification process described in Figure 1c. (c) Schematic representation of the DOPC-based pH-sensitive HPTS assay for ion transport study, employing different extravesicular salts (MCl, where M = Li, Na, K, Rb and Cs) to compare ion transport activities. (d) and (e) show Li^+ ion transport activities of $\mathbf{A_n}$ and $\mathbf{B_n}$ (n = 1-3). (f) and (g) present the ion transport selectivity of $\mathbf{A_3}$ and $\mathbf{B_3}$. (h) and (i) illustrate the determination of EC_{50} values using Hill analysis, yielding 0.65 μg/ml for $\mathbf{A_3}$ and 6.4 μg/ml for $\mathbf{B_3}$. DOPC = dioleoyl phosphatidylcholine, HPTS = 8-hydroxypyrene-1,3,6-trisulfonic acid trisodium salt.

initial temperature of 60 °C all turn out to be more active in Li^+ transport than the $\mathbf{B_n}$ series.

By varying extravesicular alkali metal chlorides, we obtained ion transport activities of 91% (Li^+), 34% (Na^+), 31% (K^+), 31% (Rb^+) and 22% (Cs^+) for $\mathbf{A_3}$ at 10 μg/ml (Figures 2f) after normalization based on their respective background values of 8.0%, 6.4%, 6.6%, 3.2%, and 10.1% (Figure S9). These comparative activity data indicate that channel $\mathbf{A_3}$ preferentially transports Li^+ ions and exhibits similar capacities in transporting Na^+, K^+, Rb^+ and Cs^+ ions. Based on these activity values, Li^+/M^+ selectivity factors were determined to be 2.7 – 4.1. Like $\mathbf{A_3}$, $\mathbf{B_3}$ also efficiently transports Li^+ (82%) but with much higher Li^+/M^+ selectivity factors of ≥ 9.2 over the other four metal ions at 25 μg/ml (Figure 2g).

For comparison, we have also examined the ion transport activities of benzene-containing **C** and naphthalene-containing **D** (Figure S8), two types of PIM variants that differ from **A** and **B** in the relative positions of their amine groups and the structural motif to which the two amine groups are attached. First, unlike **A** and **B** that exhibit good selectivity toward Li^+ ions, **C** and **D** display no selectivity in ion transport (Figure S10). Second, **C** shows minimal ion transport activity (Figure S10a), suggesting its inability to form pores of sufficiently large diameter or create multiple ion-binding and releasing sites for effective transmembrane ion transport. Third, **D** demonstrates good ion transport activity but lacks selectivity (Figure S10b), highlighting significant role played by the additional naphthalene unit in **A** and **B**.

Hill analyses of the vesicle-based kinetic data gave the EC_{50} values of 0.65 μg/ml for $\mathbf{A_3}$ (Figure 2h) and 6.4 μg/ml for $\mathbf{B_3}$ (Figure 2i), respectively, confirming their high Li^+ transport activities. We further conducted a carboxyfluorescein (CF) dye leakage assay to assess the LUV membrane integrity or potential pore formation in the presence of $\mathbf{A_3}$, $\mathbf{B_3}$, **C** and **D**. As shown in Figure S9, these PIM channels do not induce any fluorescence increase, indicating

10.1002/anie.202418304

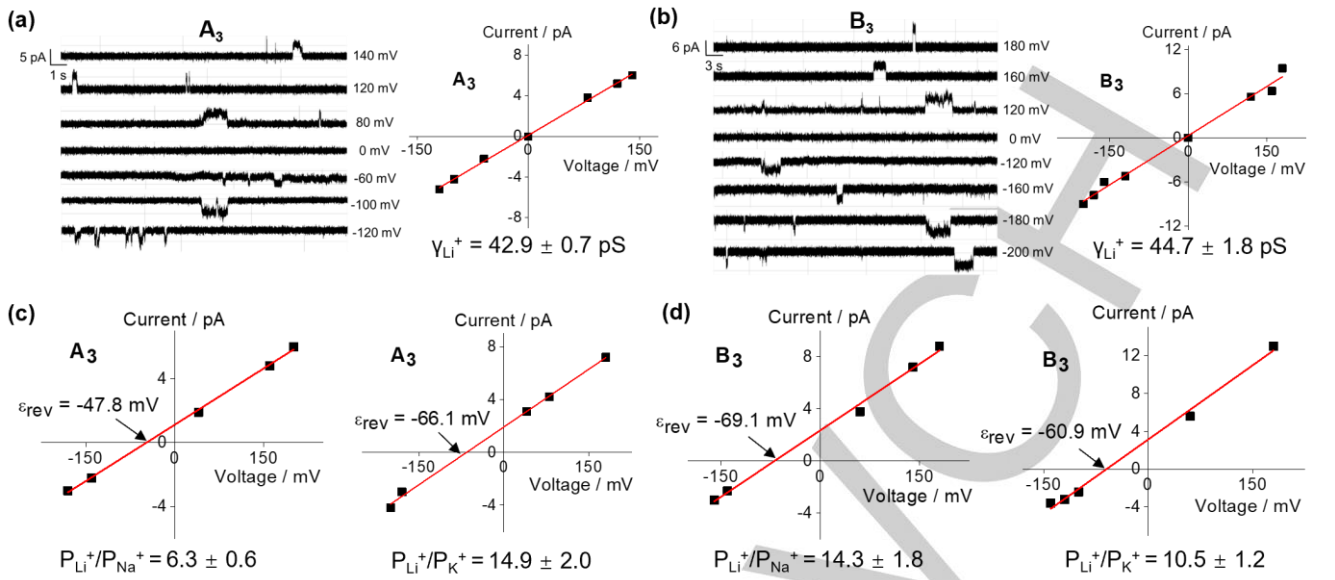

Figure 3. (a) and (b) describe single channel current traces and current–voltage (I-V) curves (*cis* chamber = *trans* chamber = 1 M LiCl) from which lithium conduction rate (γ_{Li}^+) values for **A_3** and **B_3** were determined to be 42.9 ± 0.7 pS and 44.7 ± 1.8 pS, respectively. Here, γ_{Li}^+ values were obtained by fitting the I-V curves using a linear equation of y = a + b*x where slope b is γ_{Li}^+ in the unit of nS. (c) and (d) show I-V curves (*cis* chamber = 1 M LiCl, *trans* chamber = 1 M NaCl or 1M KCl) from which the permeability ratios of P_{Li}^+/P_{Na}^+ and P_{Li}^+/P_K^+ for **A_3** and **B_3** were determined. Here, P_{Li}^+/P_M^+ values were calculated using a simplified Goldman-Hodgkin-Katz equation $\varepsilon_{rev} = RT/F \times \ln(P_M^+/P_{Li}^+)$, where R = universal gas constant (8.314 JK^{-1} mol^{-1}), T = 300 K, F = Faraday's constant (96485 $Cmol^{-1}$), and P is the ion permeability. All single channel current traces were measured in a diPhyPC-based bilayer membrane. diPhyPC = 1,2-diphytanoyl-sn-glycero-3-phosphocholine.

no CF dye leakage. Conversely, the positive control melittin, a pore-forming peptide, causes significant fluorescence increases of 55% and 100% at lower concentrations of 5 and 25 nM, respectively. These results unambiguously confirm that LUV membrane integrity is preserved in the presence of **PIM-PI** channels and that the observed ion transport activities are not due to **PIM-PI**-induced membrane-lysing effects.

To verify the ion transport mechanism of **A_3** and **B_3**, single-channel electrophysiological experiments were performed in diPhyPC-based planar lipid bilayer membrane using a planar lipid bilayer workstation (Figures 3a,b and S12).

As can be seen from Figure 3a,b, **A_3** and **B_3** both exhibit typical square signals, which clearly indicate that these **PIM-PI**s transport Li^+ via a channel mechanism. Based on the plotted current *vs* voltage (I-V) curves, the conductance rate (γ_{Li}^+) of **A_3** and **B_3** for transporting Li^+ were calculated to be 42.9 ± 0.7 pS and 44.7 ± 1.8 pS, respectively. For comparison, the two recent artificial Li^+ ion channels reported by Dong[54] and us[39] have much smaller γ_{Li}^+ values of 27.1 pS and 18.4 pS. These data confirm that these **PIM-PI** channels efficiently transport Li^+ ions at exceptionally fast rates.

To determine the ion transport selectivity of **A_3** and **B_3**, single-channel conductance measurements were conducted in asymmetrical baths (*cis* chamber = 1.0 M LiCl and *trans* chamber = 1.0 M NaCl or KCl, Figures 3c,d and S13-S16). From the plotted I-V curves for **A_3** (Figure 3c), the reverse potential values were measured as -47.8 and -66.1 mV, corresponding Li^+/Na^+ and Li^+/K^+ selectivity factors of 6.3 and 14.9, respectively. For **B_3**, the Li^+/Na^+ and Li^+/K^+ selectivity factors were determined to be 14.3 and 10.5, respectively (Figure 3d).

It is necessary to note that the ion transport selectivity factors determined using either DOPC-based LUVs or diPhyPC-based planar lipid bilayer membrane are of significant differences. Such differences might be attributed to the structural differences of the lipid molecules used, creating differential lipid bilayer membrane environments in which the sensitive **PIM-PI** channels may response in a unique way in terms of channel structure and consequently ion-transport property.

In conclusion, we have developed an interesting class of polymer-based transmembrane cation transport system using inherently porous polyimide-based **PIM-PI** channels. These channels exhibit exceptionally high Li^+ transmembrane transport activity, with Li^+ conduction rates exceeding 40 pS that is up to 1.4 times faster than the previously reported artificial Li^+ ion channels in similar lipid bilayer membrane. Moreover, we found that Li^+ transport properties can be modulated by adjusting the initial reaction temperature, resulting in higher transport activity at 60 °C and greater selectivity at 80 °C in the dioleoyl phosphatidylcholine membrane. We also observed that the channels' ion transport properties are highly dependent on the structure of membrane-forming lipid molecules used. The demonstrated channel behaviours, such as high Li^+ transport activity and selectivity, significantly broaden the functional scope of PIM materials, pioneering their application within the context of lipid bilayer membrane. Given the wide range of structural components available for building PIMs, we believe our work opens a whole new dimension of scientific research for advancing

the design and synthesis of varying types of PIM-based transmembrane ion channels. We further believe that these **PIM-PI** channels hold promise for potential applications in managing Li^+-related bipolar disorder[39] or enriching Li^+ ions from seawater or Li^+-rich salt lakes.

Acknowledgements

This work is supported by the National Natural Science Foundation of China (21602055, 22271049 and 22371048) and a start-up grant from Fuzhou University.

Conflict of Interest

The authors declare no conflict of interest.

Data Availability Statement

The data that support the findings of this study are available from the corresponding author upon reasonable request.

Keywords: Microporous Polymers • Lithium Ion Channels • Transmembrane Transport • Lithium Transport • Supramolecular Chemistry

References

[1] K. S. Thorneloe, M. T. Nelson, *Can. J. Physiol. Pharm.* **2005**, *83*, 215-242.

[2] L. W. Runnels, L. Yue, D. E. Clapham, *Science* **2001**, *291*, 1043-1047.

[3] M. A. Zaydman, J. R. Silva, J. Cui, *Chem. Rev.* **2012**, *112*, 6319-6333.

[4] E. Gouaux, R. MacKinnon, *Science* **2005**, *310*, 1461-1465.

[5] X. Zhang, W. Ren, P. DeCaen, C. Yan, X. Tao, L. Tang, J. Wang, K. Hasegawa, T. Kumasaka, J. He, J. Wang, D. E. Clapham, N. Yan, *Nature* **2012**, *486*, 130-134.

[6] L. Wang, T.-M. Fu, Y. Zhou, S. Xia, A. Greka, H. Wu, *Science* **2018**, *362*.

[7] M. Mayer, J. Yang, *Acc. Chem. Res.* **2013**, *46*, 2998-3008.

[8] N. Sakai, S. Matile, *Langmuir* **2013**, *29*, 9031-9040.

[9] F. Otis, M. Auger, N. Voyer, *Acc. Chem. Res.* **2013**, *46*, 2934-2943.

[10] J. Montenegro, M. R. Ghadiri, J. R. Granja, *Acc. Chem. Res.* **2013**, *46*, 2955-2965.

[11] T. M. Fyles, *Acc. Chem. Res.* **2013**, *46*, 2847-2855.

[12] J.-Y. Chen, J.-L. Hou, *Org. Chem. Front.* **2018**, *5*, 1728-1736.

[13] H. Gill, M. R. Gokel, M. McKeever, S. Negin, M. B. Patel, S. Yin, G. W. Gokel, *Coord. Chem. Rev.* **2020**, *412*, 213264.

[14] S.-P. Zheng, L.-B. Huang, Z. Sun, M. Barboiu, *Angew. Chem. Int. Ed.* **2021**, *60*, 566-597.

[15] K. Sato, T. Muraoka, K. Kinbara, *Acc. Chem. Res.* **2021**, *54*, 3700-3709.

[16] J. Yang, G. Yu, J. L. Sessler, I. Shin, P. A. Gale, F. Huang, *Chem* **2021**, *7*, 3256-3291.

[17] T. Yan, X. Zheng, S. Liu, Y. Zou, J. Liu, *Sci. China Chem.* **2022**, *65*, 1265-1278.

[18] A. Mondal, M. Ahmad, D. Mondal, P. Talukdar, *Chem. Commun.* **2023**, *59*, 1917-1938.

[19] L. He, T. Zhang, C. Zhu, T. Yan, J. Liu, *Chem. Eur. J.* **2023**, *29*, e202300044.

[20] M. Ahmad, S. A. Gartland, M. J. Langton, *Angew. Chem. Int. Ed.* **2023**, *62*, e202308842.

[21] J. Shen, C. Ren, H. Q. Zeng, *Acc. Chem. Res.* **2022**, *55*, 1148-1159.

[22] T. G. Johnson, M. J. Langton, *J. Am. Chem. Soc.* **2023**, *145*, 27167-27184.

[23] X. Yuan, J. Shen, H. Q. Zeng, *Chem. Commun.* **2024**, *60*, 482-500.

[24] D. M. Kim, C. M. Nimigean, *Cold Spring Harb Perspect Biol.* **2016**, *8*, a029231.

[25] L. Jin, C. Sun, Z. Li, J. Shen, H. Q. Zeng, *Chem. Commun.* **2023**, *59*, 3610-3613.

[26] H. Ma, R. Ye, L. Jin, S. Zhou, C. Ren, H. Ren, J. Shen, H. Q. Zeng, *Chin. Chem. Lett.* **2023**, 108355.

[27] T. Jiang, A. Hall, M. Eres, Z. Hemmatian, B. Qiao, Y. Zhou, Z. Ruan, A. D. Couse, W. T. Heller, H. Huang, M. O. de la Cruz, M. Rolandi, T. Xu, *Nature* **2020**, *577*, 216-220.

[28] T. Yan, S. Liu, C. Li, J. Xu, S. Yu, T. Wang, H. Sun, J. Liu, *Angew. Chem. In. Ed.* **2022**, *61*, e202210214.

[29] C. Li, Y. Wu, Y. Zhu, J. Yan, S. Liu, J. Xu, S. Fa, T. Yan, D. Zhu, Y. Yan, J. Liu, *Adv. Mater.* **2024**, *36*, 2312352.

[30] C. Lang, W. Li, Z. Dong, X. Zhang, F. Yang, B. Yang, X. Deng, C. Zhang, J. Xu, J. Liu, *Angew. Chem. Int. Ed.* **2016**, *55*, 9723-9727.

[31] C. Lang, X. Deng, F. Yang, B. Yang, W. Wang, S. Qi, X. Zhang, C. Zhang, Z. Dong, J. Liu, *Angew. Chem. Int. Ed.* **2017**, *56*, 12688-12672.

[32] F. Chen, J. Shen, N. Li, A. Roy, R. J. Ye, C. L. Ren, H. Q. Zeng, *Angew. Chem. Int. Ed.* **2020**, *59*, 1440-1444.

[33] A. Roy, H. Joshi, R. J. Ye, J. Shen, F. Chen, A. Aksimentiev, H. Q. Zeng, *Angew. Chem. Int. Ed.* **2020**, *59*, 4806-4813.

[34] C. Zhang, J. Tian, S. Qi, B. Yang, Z. Dong, *Nano Lett.* **2020**, *20*, 3627–3632.

[35] J. Shen, J. Fan, R. J. Ye, N. Li, Y. Mu, H. Q. Zeng, *Angew. Chem. Int. Ed.* **2020**, *59*, 13328-13334.

[36] J. Zhu, D. Bai, T. Yan, S. Wang, Y. Wang, J. Fu, X. Fang, J. Liu, *Angew. Chem. Int. Ed.* **2020**, DOI: 10.1002/anie.201916755.

[37] S. Qi, J. Tian, J. Zhang, L. Zhang, C. Zhang, Z. Lin, J. Min, S. Mao, Z. Dong, *CCS Chem.* **2022**, *4*, 1850-1857.

[38] J. Shen, R. Ye, Z. Liu, H. Q. Zeng, *Angew. Chem. Int. Ed.* **2022**, *61*, e202200259.

[39] J. Shen, D. R, Z. Li, H. Oh, H. Behera, H. Joshi, M. Kumar, A. Aksimentiev, H. Q. Zeng, *Angew. Chem. Int. Ed.* **2023**, *62*, e202305623.

[40] A. Roy, J. Shen, H. Joshi, W. Song, Y.-M. Tu, R. Chowdhury, R. Ye, N. Li, C. Ren, M. Kumar, A. Aksimentiev, H. Q. Zeng, *Nat. Nanotech.* **2021**, *16*, 911-917.

[41] J. Shen, A. Roy, H. Joshi, L. Samineni, R. J. Ye, Y.-M. Tu, W. Song, M. Skiles, M. Kumar, A. Aksimentiev, H. Q. Zeng, *Nano Lett.* **2022**, *22*, 4831–4838.

[42] N. B. McKeown, P. M. Budd, *Chem. Soc. Rev.* **2006**, *35*.

[43] N. B. McKeown, *Sci. China Chem.* **2017**, *60*, 1023-1032.

[44] N. B. McKeown, *Polymer* **2020**, *202*.

[45] P. M. Budd, B. S. Ghanem, S. Makhseed, N. B. McKeown, K. J. Msayib, C. E. Tattershall, *Chem. Commun.* **2004**.

[46] M. Carta, M. Croad, K. Bugler, K. J. Msayib, N. B. McKeown, *Polymer Chem.* **2014**, *5*.

10.1002/anie.202418304

Research Communications

[47] Y. Wang, N. B. McKeown, K. J. Msayib, G. A. Turnbull, I. D. W. Samuel, *Sensors* **2011**, *11*, 2478-2487.

[48] X. Weng, J. E. Baez, M. Khiterer, M. Y. Hoe, Z. Bao, K. J. Shea, *Angew. Chem. In. Ed.* **2015**, *54*, 11214-11218.

[49] M. Carta, R. Malpass-Evans, M. Croad, Y. Rogan, J. C. Jansen, P. Bernardo, F. Bazzarelli, N. B. McKeown, *Science* **2013**, *339*, 303-307.

[50] Z.-X. Low, P. M. Budd, N. B. McKeown, D. A. Patterson, *Chem. Rev.* **2018**, *118*, 5871-5911.

[51] Y. Wang, X. Ma, B. S. Ghanem, F. Alghunaimi, I. Pinnau, Y. Han, *Mater. Today Nano* **2018**, *3*, 69-95.

[52] M. Usman, A. Ahmed, B. Yu, Q. Peng, Y. Shen, H. Cong, *Eur. Polymer J.* **2019**, *120*.

[53] H. W. H. Lai, F. M. Benedetti, J. M. Ahn, A. M. Robinson, Y. Wang, I. Pinnau, Z. P. Smith, Y. Xia, *Science* **2022**, *375*, 1390-1392.

[54] L. Zhang, C. Zhang, X. Dong, Z. Dong, *Angew. Chem. Int. Ed.* **2023**, *62*, e202214194.

[55] X. Ma, I. Pinnau, *Macromolecules* **2018**, *51*, 1069-1076.

[56] J. Mahler, I. Persson, Inorg. Chem. **2012**, *51*, 425.

10.1002/anie.202418304

WILEY-VCH

Research Communications

Entry for the Table of Contents

PIM-Based Li^+ Channels

Fei Gou, Qiuting Wang, Zihong Yang, Wenju Chang, Jie Shen and Huaqiang Zeng**

_____ ***Page – Page***

Artificial Lithium Channels Built from Polymers with Intrinsic Microporosity

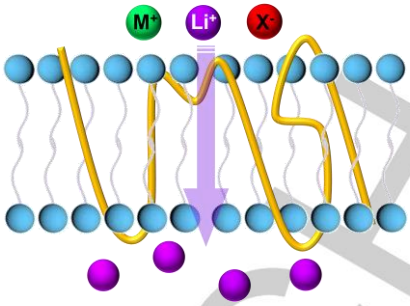

Polymers with intrinsic microporosity have been used to construct artificial lithium channels. Record-high transmembrane Li^+ transport rates (γLi^+ > 40 pS) and high Li^+ transport selectivity relative to both Na^+ and K^+ ions (selectivity > 10) have been determined using these ion channels. The transport properties can be tuned by adjusting the temperature at which the microporous polymers are synthesized.